A THESIS SUBMITTED TO
THE GRADUATE SCHOOL OF NATURAL AND APPLIED SCIENCES
OF ÇANKIRI KARATEKİN UNIVERSITY

DETERMINATION OF NON-ISOTHERMAL REDUCTION KINETICS OF GÖRDES LATERITE ORE-TUNÇBİLEK LIGNITE COAL MIXTURE BY THERMAL GRAVIMETRY

IN PARTIAL FULFILLMENT OF THE REQUIREMENTS
FOR
THE DEGREE OF MASTER OF SCIENCE
IN
CHEMICAL ENGINEERING

BY

RAND SAAD AHMAD NAJE AHMAD NAJE

ÇANKIRI

2023

DETERMINATION OF NON-ISOTHERMAL REDUCTION KINETICS OF GÖRDES LATERITE ORE-TUNÇBİLEK LIGNITE COAL MIXTURE BY THERMAL GRAVIMETRY

By Rand Saad Ahmad Naje Ahmad NAJE

June 2023

We certify that we have read this thesis and that in our opinion it is fully adequate, in scope and in quality, as a thesis for the degree of Master of Science.

Advisor **:** Assoc. Prof. Dr. Nesibe DİLMAÇ

Examining Committee Members:

Chairman **:** Assoc. Prof. Dr. Nesibe DİLMAÇ
Chemical Engineering
Çankırı Karatekin University

Member **:** Assoc. Prof. Dr. Mehmet Selçuk MERT
Energy Systems Engineering
Yalova University

Member **:** Assist. Prof. Dr. Semahat DORUK
Chemical Engineering
Çankırı Karatekin University

Approved for the Graduate School of Natural and Applied Sciences

Prof. Dr. Hamit ALYAR
Director of Graduate School

I hereby declare that all information in this document has been obtained and presented in accordance with academic rules and ethical conduct. I also declare that, as required by these rules and conduct, I have fully cited and referenced all material and results that are not original to this work.

Rand Saad Ahmad Naje Ahmad NAJE

ABSTRACT

DETERMINATION OF NON-ISOTHERMAL REDUCTION KINETICS OF GÖRDES LATERITE ORE-TUNÇBİLEK LIGNITE COAL MIXTURE BY THERMAL GRAVIMETRY

Rand Saad Ahmad Naje Ahmad NAJE

Master of Science in Chemical Engineering

Advisor: Assoc. Prof. Dr. Nesibe DİLMAÇ

June 2023

In this study, fine laterite samples from Manisa Gördes mine were calcined, and mixed with dried and fine Tunçbilek lignite particles in molar stoichiometric ratio (87% laterite and 13% lignite). Afterwards, the mixtures were heated from ambient temperature to 1000 ºC under N_2 flow at different heating rates; 5, 10, 15, 25, and 40 ºC/min in a thernogravimetric analyser. All experiments were repeated for the same amount of lignite keeping all other parameters the same. Using the weight loss values of both lignite and mixture samples, reduction degrees of the metallic oxides in the ore samples were calculated. Due to the low concentration of the lignite in the mixtures, the highest reduction degree was around 29%. The obtained data was analyzed by non-isothermal kinetic methods and the mean activation energy (E_a) for 0 to 0.18 conversion range of the reduction was determined as 107.97 kJ/mole, 51.87 kj/mole, and 63.67 kj/mole via Friedman (FR), Flynn-Wall-Ozawa (FWO), and Kissinger-Akahira-Sunose (KAS) methods, respectively. On the other hand, Coats-Redfern (CR) method revealed that the initial stage of the reduction of calcined Gördes laterite by Tunçbilek lignite between 0 and 0.29 conversion range progressed under phase boundary chemical reaction control with E_a of 54.04 kJ/mole.

2023, 35 pages

Keywords: Laterite, Lignite, Carbothermic reduction, Non-isothermal reaction kinetics, Thermal gravimetry.

ÖZET

GÖRDES LATERİT CEVHERİ-TUNÇBİLEK LİNYİT KÖMÜRÜ KARIŞIMININ İZOTERMAL OLMAYAN İNDİRGENME KİNETİĞİNİN TERMAL GRAVİMETRİ YOLUYLA BELİRLENMESİ

Rand Saad Ahmad Naje Ahmad NAJE
Kimya Mühendisliği, Yüksek Lisans
Tez Danışmanı: Doç. Dr. Nesibe DİLMAÇ
Haziran 2023

Bu çalışmada, Manisa Gördes madeninden temin edilen, tanecik boyutu 100 µm' den küçük olan ince laterit numuneleri öncelikle kurutulmuş, ardından 900 ºC kül fırınında 18 saat boyunca kalsine edilmiştir. Kalsine cevher numuneleri, kurutulmuş ve yine tanecik boyutu 100 µm' den küçük olan ince Tunçbilek linyiti ile molar stokiyometrik oranda (%87 laterit ve %13 linyit) karıştırılmıştır. Karışımlar bir termal gravimetrik analiz cihazında N_2 akışı altında 5, 10, 15, 25 ve 40 ºC/dak. ısıtma hızlarında ortam sıcaklığından 1000 ºC' ye kadar ısıtılarak cevher ve linyit karışımlarının izotermal olmayan indirgenme sürecine ait ağırlık değişimi izlenmiştir. Tüm deneyler, diğer tüm parametreler aynı tutularak aynı miktarda linyit için tekrarlanmış ve linyitin izotermal olmayan şartlardaki ağırlık değişimi de kaydedilmiştir. Hem linyit, hem de karışım numunelerinin ağırlık kaybı değerleri kullanılarak cevher numunelerindeki metalik oksitlerin indirgenme dereceleri hesaplanmıştır. Karışımlardaki linyit konsantrasyonunun düşük olması nedeniyle en yüksek indirgeme derecesi %29 civarında olmuştur. Elde edilen veriler izotermal olmayan kinetik yöntemlerle analiz edilmiş ve indirgemenin 0 ila 0,18 dönüşüm aralığında kalan kısmı için ortalama aktivasyon enerjisi (E_a) Friedman (FR), Flynn-Wall-Ozawa (FWO) ve Kissinger-Akahira-Sunose (KAS) yöntemleri ile sırasıyla 107,97 kJ/mol, 51,87 kj/mol ve 63,67 kJ/mol olarak belirlenmiştir. Coats-Redfern (CR) yöntemi ise, kalsine Gördes lateritinin Soma linyiti ile indirgenmesinin 0 ile 0,29 dönüşüm aralığında kalan ilk aşamasının, "$g(\alpha)=\alpha= k_i.t$" denklemi ile karakterize edilen, faz sınırında kimyasal reaksiyon kontrolü altında ilerlediğini ortaya koymuştur. Özetle, ince kalsine Gördes lateritinin ince

Tunçbilek kömürü ile termal analiz cihazında izotermal olmayan indirgenme prosesine ait kinetik triplet (model denklemi, aktivasyon enerjisi ve Arrhenius frekans faktörü) sırasıyla F0, 54,04 kJ/mol, ve 0,49 l^{n-1}. mol $^{1-n}$ .s^{-1} olarak belirlenmiştir.

2023, 35 sayfa

Anahtar Kelimeler: Laterit, Linyit, Karbotermik indirgeme, İzotermal olmayan reaksiyon kinetiği, Termal gravimetri.

PREFACE AND ACKNOWLEDGEMENTS

I would like to express my deepest thanks to my esteemed advisor Associate Professor Dr. Nesibe DİLMAÇ for her great efforts and patience. Also, I would like to thank to Associate Professor Dr. Ömer Faruk DİLMAÇ for his technical assistance. Finally, I would like to thank my beloved family who have been by my side in every moment of my life for their patience, sacrifice and support.

Rand Saad Ahmad Naje Ahmad NAJE
Çankırı-2023

CONTENTS

LIST OF SYMBOLS

T	Absolute Temperature (K)
E_a	Activation Energy (kJ/mol)
A	Arrhenius Frequency Factor (l^{n-1}. mol^{1-n}. s^{-1})
f(α)	Differantial Model Equation (-)
g(α)	Integral Model Equation (-)
k(T)	Rate Constant (l^{n-1}. mol^{1-n}. s^{-1})
α	Reduction Degree or Reaction Extend (-)
R	Universal Gas Constant (8.314 J/mol.K)

LIST OF ABBREVIATIONS

CR	Coats-Redfern Method
EV	Electric Vehicle
FR	Friedman Method
FWO	Flynn-Wall-Ozawa Method
HPAL	High Pressure Acid Leaching
KAS	Kissinger-Akahira-Sunose Method
RKEF	Rotary Kiln Electric Furnace
TGA	Thermal Gravimetric Analysis
TMA	Thermal Mechanical Analysis
XRF	X-Ray Fluorescence

LIST OF FIGURES

LIST OF TABLES

1. INTRODUCTION

1.1 Nickel

Nickel (Ni) is a hard and shiny transition metal (Figure 1.1) that takes place in Group 10 of the periodic table, with an atomic number of 28 and an atomic weight of 58.69 g/mol. It is the fifth most abundant element on Earth, yet it is more concentrated towards the core compared to the Earth's crust. Its name comes from an old Saxon term "kupfernickel". When it was first discovered as niccolite (nickel arsenide mineral) by 16th-century German miners in the Ore Mountains, it led to the misconception that a new type of copper ore had been discovered because of its pale brown-red appearance. However, the miners failed to extract copper from that rock, and they blamed "Nickel", a mischievous demon from German mythology for besetting the copper in the ore. Therefore, that newly discovered ore was named "kupfernickel" *i.e*. devil's copper.

Figure 1.1 10×10×10 mm polished Ni cube with 99.6% purity (EBAY 2023)

About a century later (1751), Baron Axel Fredrik Cronstedt -a Swedish chemist-, reattempted to extract copper from "kupfernickel" by heating it with charcoal, but he realized that the obtained metal exhibited distinctive properties (such as being white, and magnetic) which revealed that it was not copper. Thus, after dropping "kupfer", nickel was isolated and classified as a private element for the first time.

As seen in Figure 1.2, Ni has eminent physical and chemical properties that make it essential for the production of thousands of products from coins to wind turbines (LIVESCIENCE 2023, NICKEL INSTITUTE 2023, WIKIPEDIA 2023). It alloys with other metals easily, exhibits superior catalytic properties, and melts at a relatively high temperature (1453 ºC) compared to other common metals, such as aluminum (660 ºC), silver (962 ºC), gold (1064 ºC), copper (1085 ºC), and cast iron (1204 ºC). It is highly ductile, malleable, and resistant to oxidation, corrosion, and heat. Due to these properties, it is mostly coated or electroplated onto other materials (especially onto the softer metals and plastics) to form a protective coating (PUBCHEM 2023). Moreover, it is one of only four elements (cobalt, nickel, iron, and gadolinium) that are ferromagnetic at room temperature (BRITANNICA 2023), and it can be fully recycled many times without any loss in its quality.

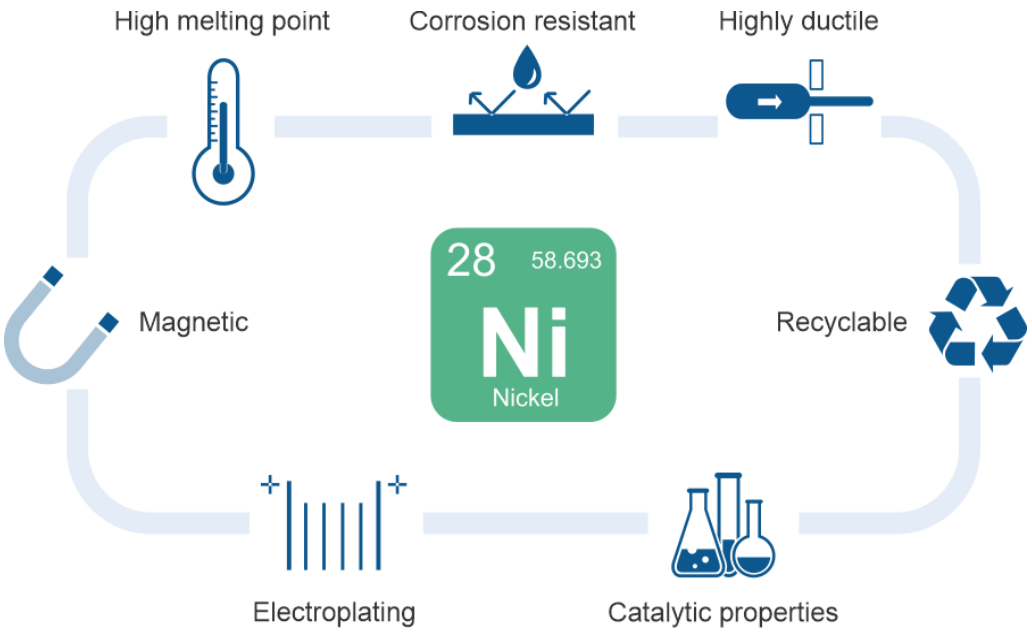

Figure 1.2 Main properties of Ni (NICKELSEARCH 2023)

1.2 Utilization Areas of Nickel and Its Alloys

Ni is mostly used as its alloys rather than its pure metallic form since it is more functional and valuable in this way. The alloys are either used in manufacturing processes or transformed into integrated products. Thus nickel compounds are never directly accessible to users. Probably due to this reason, the importance of nickel compounds is not adequately appreciated although they are utilized in countless products (NICKEL INSTITUTE 2023). However, the widespread use of electric vehicles (EVs) will inevitably increase the importance of nickel, which is one of the most important battery materials, soon (Yang *et al.* 2016, Elliott and Pickles 2017, Wang *et al.* 2017, Lv *et al.* 2018, Li *et al.* 2018, Zhu *et al.* 2019, Zhang *et al.* 2020). Figure 1.3 shows the main utilization areas of nickel and its compounds by percentage.

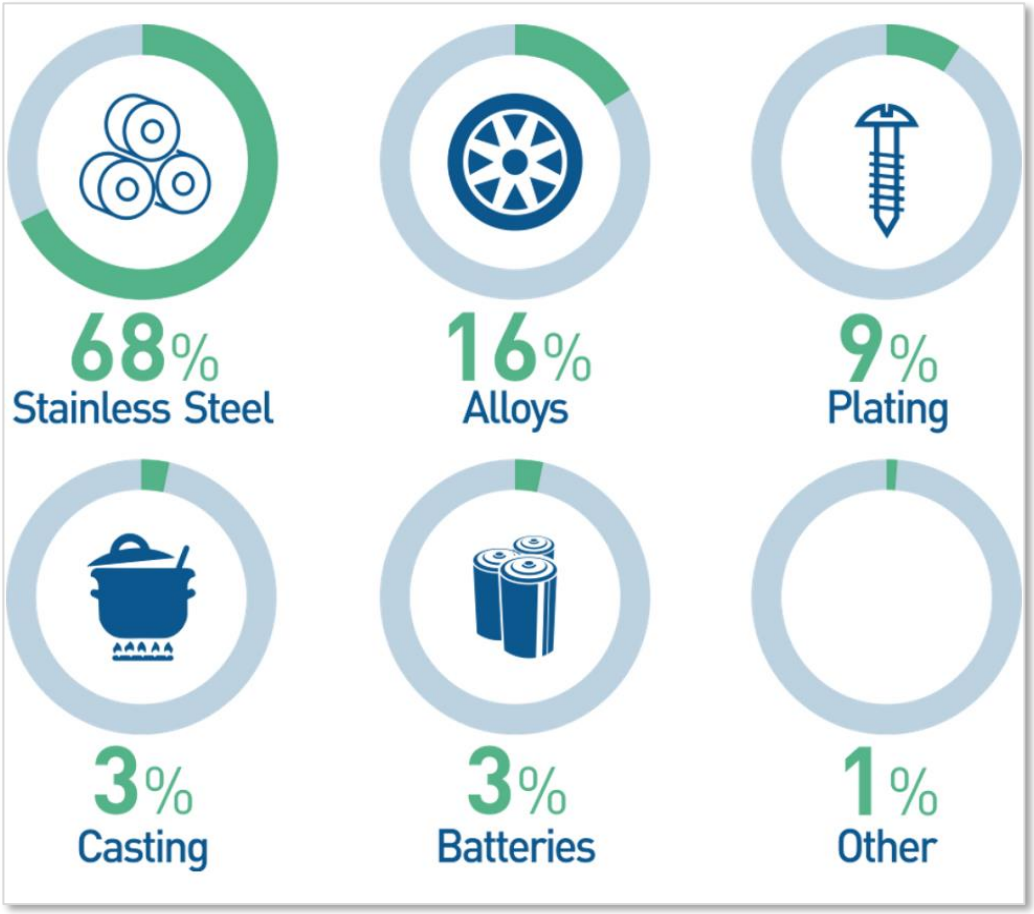

Figure 1.3 Utilization areas of Ni and its compounds (NICKELSEARCH 2023)

Stainless steel production is by far the largest consumer of Ni with a share of 68%. Although it is a relatively new member of the materials world, stainless steel has revolutionized our modern world in 100 years, as it is chemically and mechanically durable, inexpensive, formable, and weldable. Almost every manufacturing sector -from catering equipment and healthcare to the construction and automotive industries- utilizes steel. However, since the requirements differ from one sector to another, the properties and compositions of the steels also differ. Several types of steels are produced by adding different ferroalloys or alloying elements (at least 11% chromium, manganese, molybdenum, nickel, 0.1%-2.5% carbon, etc.) to the composition. Nickel is one of those elements as seen in Figure 1.4, and has a key role in steel production. It mainly offsets the undesired side effects of chromium -the must of steel- such as reducing hardness and creating steel ferromagnetism (PIPINGMART 2023).

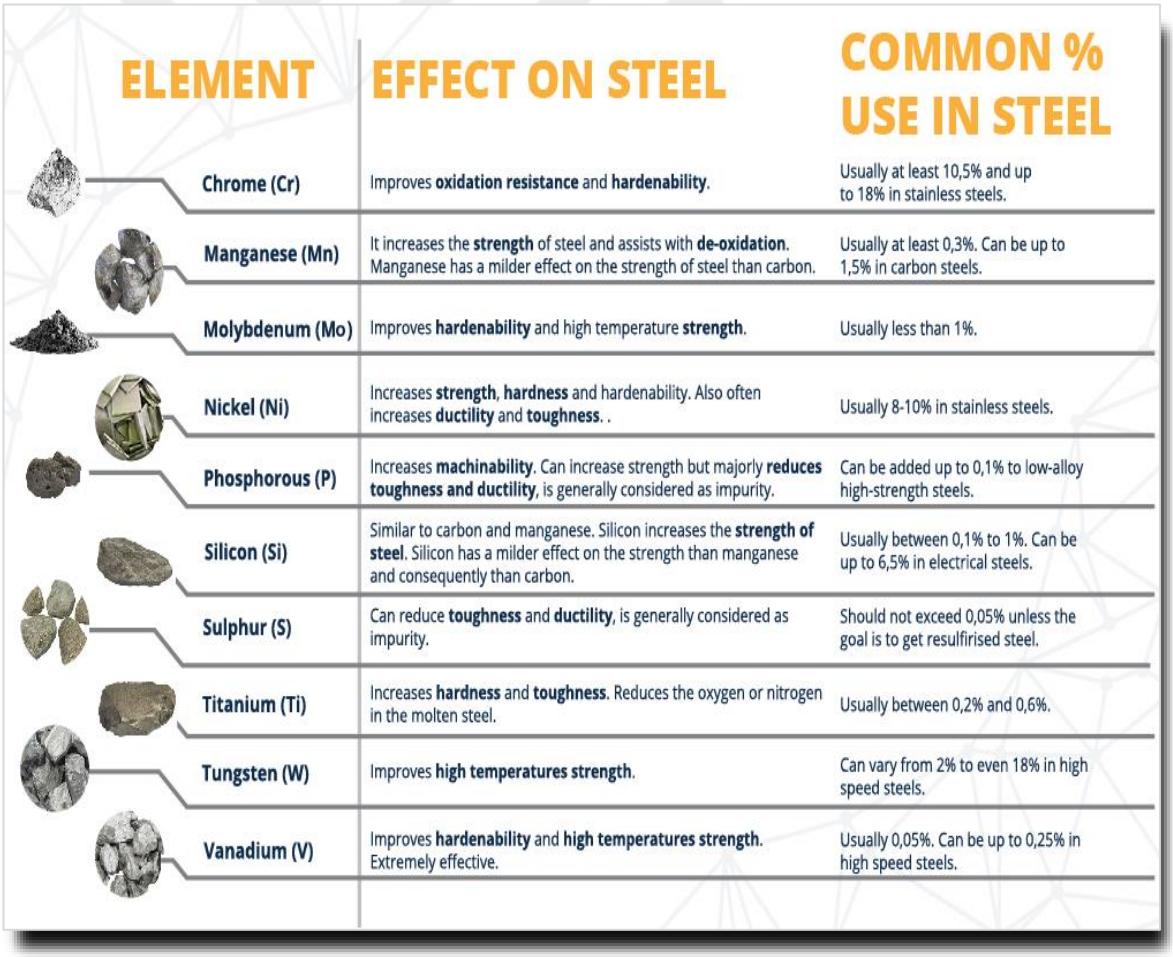

ELEMENT	EFFECT ON STEEL	COMMON % USE IN STEEL
Chrome (Cr)	Improves **oxidation resistance** and **hardenability**.	Usually at least 10,5% and up to 18% in stainless steels.
Manganese (Mn)	It increases the **strength** of steel and assists with **de-oxidation**. Manganese has a milder effect on the strength of steel than carbon.	Usually at least 0,3%. Can be up to 1,5% in carbon steels.
Molybdenum (Mo)	Improves **hardenability** and high temperature **strength**.	Usually less than 1%.
Nickel (Ni)	Increases **strength**, **hardness** and hardenability. Also often increases **ductility** and **toughness**. .	Usually 8-10% in stainless steels.
Phosphorous (P)	Increases **machinability**. Can increase strength but majorly **reduces toughness and ductility**, is generally considered as impurity.	Can be added up to 0,1% to low-alloy high-strength steels.
Silicon (Si)	Similar to carbon and manganese. Silicon increases the **strength of steel**. Silicon has a milder effect on the strength than manganese and consequently than carbon.	Usually between 0,1% to 1%. Can be up to 6,5% in electrical steels.
Sulphur (S)	Can reduce **toughness** and **ductility**, is generally considered as impurity.	Should not exceed 0,05% unless the goal is to get resulfirised steel.
Titanium (Ti)	Increases **hardness** and **toughness**. Reduces the oxygen or nitrogen in the molten steel.	Usually between 0,2% and 0,6%.
Tungsten (W)	Improves **high temperatures strength**.	Can vary from 2% to even 18% in high speed steels.
Vanadium (V)	Improves **hardenability** and **high temperatures strength**. Extremely effective.	Usually 0,05%. Can be up to 0,25% in high speed steels.

Figure 1.4 Common alloying elements used in steelmaking (METALS-HUB 2023)

Alloy production is the second massive consumer of Ni (16%) since adding Ni to other metals significantly improves the physical and mechanical properties of the produced material, particularly the strength and the resistance to corrosion. For example, Ni-alloyed copper pipes are used in desalination plants in which seawater is converted into fresh water, while Ni-alloyed steel is used for making armor plates, burglar-proof vaults, automotive gearboxes, and other machine parts.

Alnico® magnets -a very powerful permanent magnet family- are made from alloys of aluminum, nickel, cobalt, and iron.

Permalloy® is a highly magnetic nickel, iron, and molybdenum alloy which is widely used for fabricating thin pieces that are laminated to form transformer cores.

Nickel-chromium alloys (Nichrome® and Constantan®) are commonly used for manufacturing resistance wires, and heating elements for hair dryers, toasters, heat guns, and space heaters. These wires are also used by ceramic artists to make skeletons which help sculptures to hold their shapes while they are still soft and cope with high temperatures when the artwork is fired in a kiln.

Superalloys of Ni (Invar®, Monel®, Inconel®, and Hastelloy®) can withstand extreme temperatures and harsh environments, and they keep their surface stability, toughness, and creep resistance at challenging conditions. Because of these characteristics, they are widely used in jet and rocket engines, aerospace, marine, and automotive industries, highly specialized military productions, offshore installations, nuclear power and chemical processing plants, and power generation turbines.

The third sector where nickel is widely used is plating. From its identification as an element in 1751 until the discovery of stainless steel in 1912, Ni was primarily used in coinage and plating to add luster, reduce weight, and increase the wear and corrosion resistance of the material. For example, "German silver" (a nickel, copper, and zinc alloy which is more commonly known as "nickel silver") was named for its silvery

shine appearance although it does not contain any silver. However, prolonged contact with Ni plated items such as piercings, jewelry, watches, and coins caused an itchy skin condition named "contact dermatitis" over the years (Mcllveen and Negusanti 1994). Thus, European Union (EU) regulated the limits for Ni utilization by legislations EN12472 and EN1811. Taking into account the above-mentioned health problems and the fair adhesion properties of Ni together, the utilization of it as a sub-coating *i.e.* under coat for subsequent coating layers such as chrome, became more favorable instead of utilization as a top coating.

The newest but fastest-growing sector that needs Ni is battery manufacturing. Ni is an essential ingredient in this sector since the 1980s. The first-generation portable devices such as digital cameras, and walkmans relied almost only on nickel-cadmium (NiCd) batteries. However, by the 1990s, nickel-metal-hydride (NiMH) batteries took over the reign to solve the toxicity problem caused by NiCd cells. The recent utilization of Ni is constituting the cathode of the lithium-ion batteries which power everyday devices like mobile phones, laptops, and all other rechargeable households. It seems like the global Ni demand for lithium-ion batteries will increase due to the prevalence of electric vehicles (EVs). Brazilian mining company Vale (VALE3.SA) has predicted a 44% jump in nickel demand by 2030 from 2022 levels due to the high demand for batteries meant for EVs (REUTERS 2023).

Nickel is also essential for manufacturing the most widely used catalysts in the fuel, food, fertilizers, and fine chemicals industries. For example, hydrogenation of vegetable oils, steam reforming, hydrotreating, and catalytic cracking processes all require Ni catalysts. Many indispensable compounds of modern daily life, such as foods, pharmaceuticals, agrochemicals, fibers, fragrances, and personal care products are produced from building-block chemicals via these catalysts.

Apart from the abovementioned sectors, Ni oxides are used as raw material in the production of inorganic pigments and fritz in ceramic glazes. Moreover, when used in sunglasses, nickel oxide performs as a colorant, gives a brown tint to absorb sunlight, and hence protects the eye against UV radiation.

1.3 Nickel Sources

There are two main nickel sources, the sulfides and the laterites. Figure 1.5 shows the distribution of global sulphite and laterite ore deposits (Elias 2002). Laterite ores are more concentrated in South-East Asia, whilst sulphide deposits are mostly found in South Africa, Canada, Russia, and Australia (Zhou, 2005).

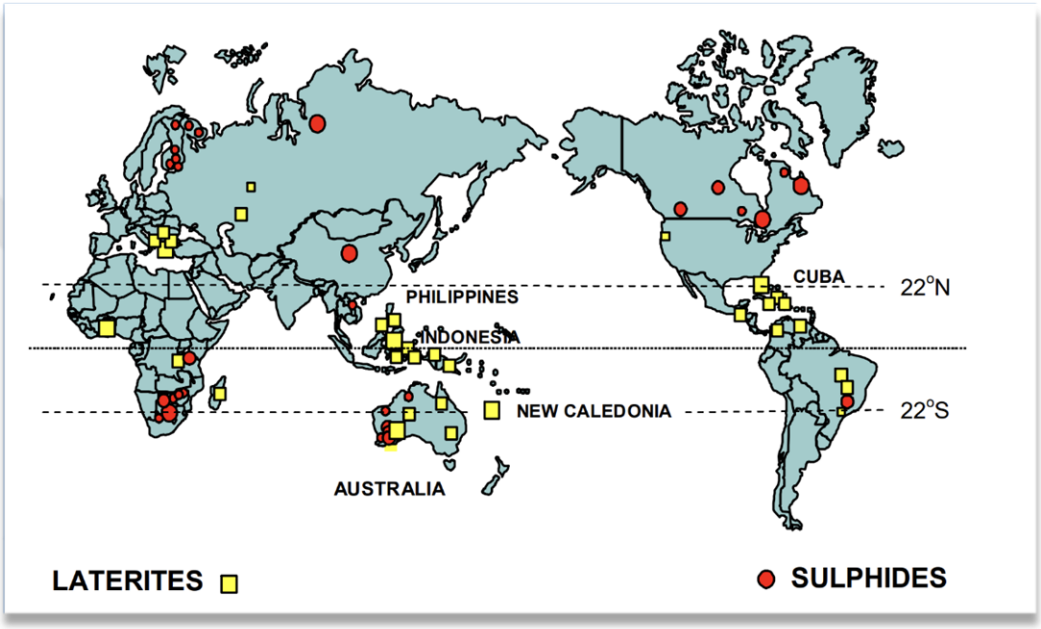

Figure 1.5 Global distribution of nickel laterite and sulphide deposits (Elias 2002)

70% of Ni reserves are lateritic, but they are not preferable as a primary source for Ni production since the low grade and the complex mineralogy of laterites makes extraction of Ni costly and highly energy consuming. On the other hand, Ni in sulfide ores can be easily enriched and recovered, thus 60% of global Ni production is derived from sulfide ores. However, the sulphide reserves are depleting due to the excessive utilization over years. For this reason, the industry is switching to extracting Ni from laterite ores (Valix *et al*. 2001, Zhai *et al.* 2009, Norgate and Jahanshahi 2011). Figure 1.5 exhibits major types of lateritic and sulfide ores, processing options and final products.

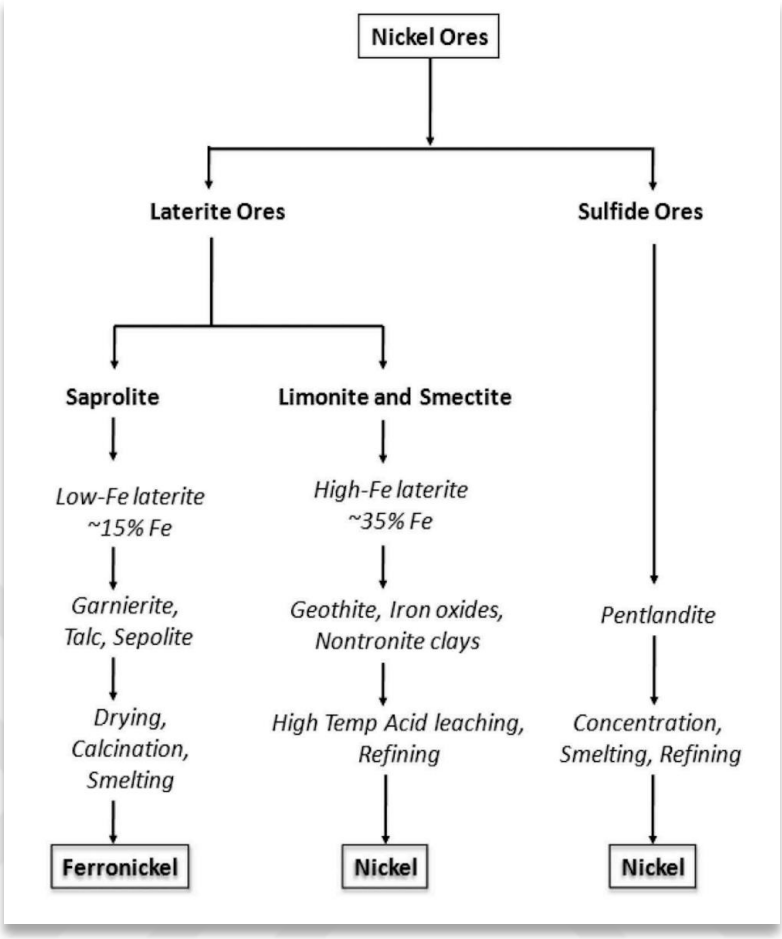

Figure 1.6 Major types of Ni ores, processing options and final products (Meshram *et al.* 2019)

1.4 Nickel Market and Production Processes

As Ni is a highly demanded metal for battery production and a vital component for stainless steel manufacturing, countries and companies are eager to take a larger share of global Ni production. In 2020, world nickel production eventuated as 2.5 million tons despite the global epidemic, whilst the supply is estimated to reach 3.7 million tons in 2023 (Figure 1.7).

Today's nickel market is a US$20+ billion per year industry and it is likely to enlarge in the near future since the EVs sector grows exponentially. This will inevitably lead to an increase in Ni mining. Figure 1.8 illustrates the top 10 Ni mining companies around the world according to the 2020 productions (kt).

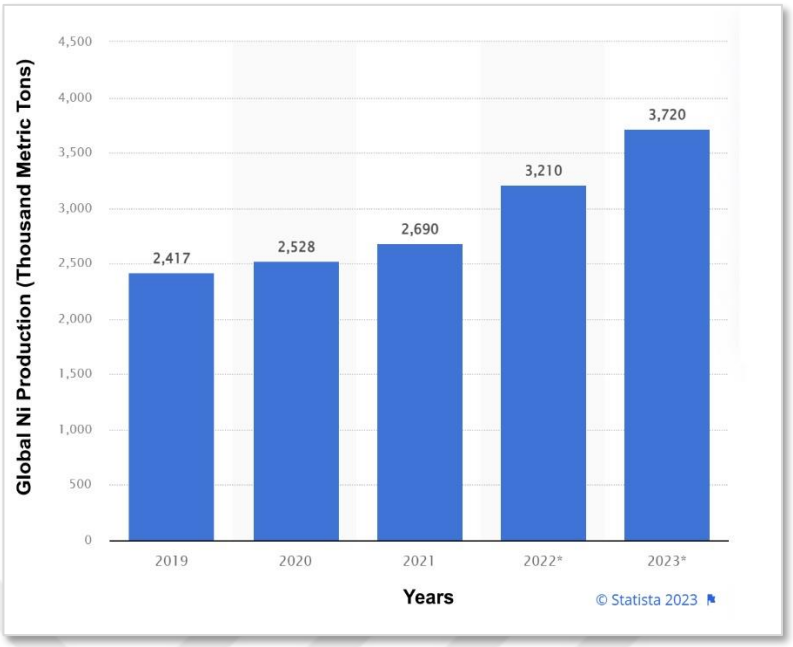

Figure 1.7 Global Ni production by years (STATISTA 2023)

Figure 1.8 Top 10 Ni mining companies by 2020 production (ELEMENTS 2023)

The conventional flotation and fine grinding technologies are unappropriate for laterites. Thus, they can be processed by a number of different methods such as hydrometallurgical, pyrometallurgical, and combined processes (atmospheric leaching, high-pressure acid leaching (HPAL)), reductive roasting followed by ammonia leaching (Caron process), rotary kiln electric furnace process (RKEF or Elkem process), and direct reduction followed by magnetic separation process (Dilmaç 2021).

Since the composition of laterites varies according to the ore content and the physical properties of the sediment, the production technology is determined based on these properties. Table 1.1 and Figure 1.9 show typical laterite ore types and their processing techniques (Liu 2002).

Table 1.1 Processing technologies for various laterite ores (Liu 2002)

Ore type	Chemical composition %					Processing technology
	Ni	Co	Fe	Cr_2O_3	MgO	
Limonite	0.8-1.5	0.1-0.2	40-50	2-5	0.5-5	Hydro
	1.5-1.8	0.02-0.1	25-40	1-2	1-15	Pyro or Hydro
Saprolite	1.8-3	0.02-0.1	10-25	1-2	15-35	Pyro

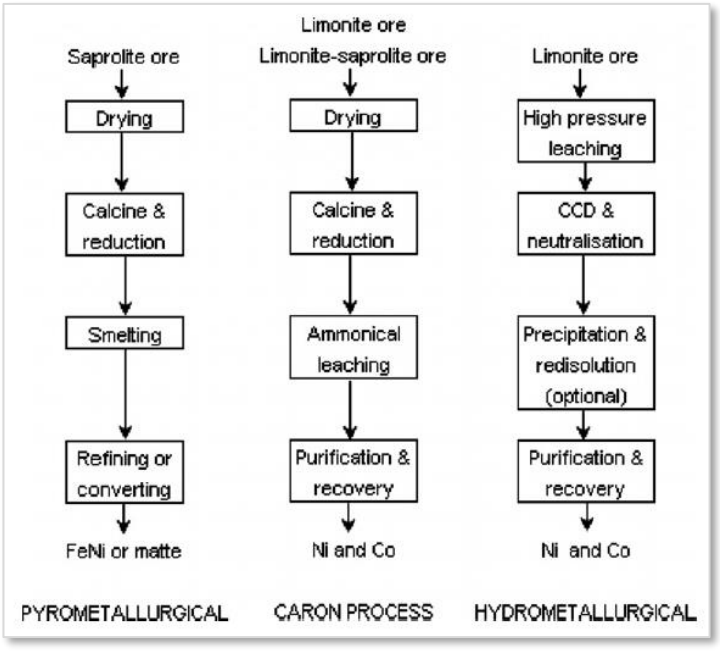

Figure 1.9 Main Ni production processes from laterites (Norgate and Jahanshahi 2011)

1.5 Thermal Gravimetric Analysis (TGA)

Thermal analysis is a set of techniques that examines the change of any physical property of a substance as a function of temperature, in which a controlled heating program is applied. The technique is named according to the property studied. For example, if the variation of the sample weight with increasing temperature is examined; it is referred as thermal gravimetric analysis (TGA), whilst the variation of sample sizes with increasing temperature is examined, the technique is referred as dilatometry, and if the change of the mechanical properties of the sample with increasing temperature is examined, the method is named as thermal mechanical analysis (TMA).

Since the weight changes measured by TGA includes low heat and mass transfer effects, the method gives reliable information about pure kinetics of the reaction mechanism. This makes TGA an efficient, powerful and versatil method which is preferred for a wide variety of kinetic studies for many years.

Nonisothermal or linear heating rate TGA method involves heating the material to a desired temperature at a desired constant heating rate with time and it has been shown to be very useful and one of the best methods for studying the reaction kinetics (Emiola-Sadiq *et al.* 2021).

1.6 Non-Isothermal Kinetics of Laterite Reduction

The reduction of laterite by a solid reductant (such as coal carbon) takes place according to the reaction given in Equation (1.1).

$$NiFe_2O_4 \ + \ 2\mathrm{C} \rightarrow \mathrm{Ni} + 2\mathrm{Fe} + 2\mathrm{CO}_2 \qquad (1.1)$$

The conversion or reduction degree (α) of the metal oxides (iron and nickel oxides) in the laterite at any "t" moment of a given nonisothermal reduction run can be calculated with the help of Equation (1.2).

$$\alpha = \frac{m_o - m_t}{m_o - m_r} \tag{1.2}$$

In this equation, "m_o" is the mass of the ore in the fully oxidized state, "m_t" is the mass of the ore at any time "t", "m_r" is the mass of the ore in the fully reduced state (Dilmaç 2021, AlSalihi 2022).

As is known, the rate (dα/dt) of any gas-solid reaction (especially when the reductant is solid) is expressed by Equation (1.3) in which "k(T)" is the temperature dependent reaction rate constant, and "f(α)" is the differential model function describing the reaction mechanism (Su *et al*. 2017, Farooqui *et al.* 2018, Fedunik-Hofman *et al.* 2019).

$$\frac{d\alpha}{dt} = k(T).f(\alpha) \tag{1.3}$$

If Arrhenius Equation is inserted into the right-hand side, and linear heating rate (β = dT/dt) is inserted into the left-hand side of Equation (1.3), Equation (1.4) is obtained. It should be noted that "A" is the pre-exponential factor, "R" is the universal gas constant, "E_a" is the activation energy, and "T" is the absolute temperature in Equation (1.4).

$$\beta.\frac{d\alpha}{dT} = A.e^{\left(-E_a/R.T\right)}.f(\alpha) \tag{1.4}$$

If Equation (1.4) is rearranged, Equation (1.5) (in which "g(α)" is the integral model function describing the reaction mechanism) is obtained.

$$g(\alpha) = \int_0^{\alpha} \frac{d\alpha}{f(\alpha)} = \int_0^{T} \frac{A}{\beta}.e^{\left(-E_a/R.T\right)}.dT \tag{1.5}$$

"E_a/RT" in Equation (1.5) can be replaced with "u" to express "g(α)" in a more general form as in Equation (1.6).

$$g(\alpha) = \frac{A.E_a}{\beta.R}\int_{\infty}^{u}\left(\frac{e^{-u}}{u^2}\right).du = \frac{A.E_a}{\beta.R}.p(u) \quad (1.6)$$

"p(u)" seen in Equation (1.6) is the "temperature or exponential integral" and it can solely be obtained by using various algebraic approximations because it has no analytical solution for nonisothermal conditions (Dilmaç 2021).

The most common f(α) and g(α) functions used in gas-solid reaction kinetics are given in Table 1.2.

Table 1.2 The most common f(α) and g(α) functions for gas-solid reactions

Reaction Model	**Symbol**	**$f(\alpha)=(1/k_i).(d\alpha/dt)$**	**$g(\alpha)=k_i.t$**
One-dimensional diffusion model	$D_1(\alpha)$	$1/(2\alpha)$	α^2
Two-dimensional diffusion model	$D_2(\alpha)$	$(-\ln(1-\alpha))^{-1}$	$(1-\alpha)\ln(1-\alpha)+\alpha$
Three-dimensional diffusion model (Jander equation)	$D_3(\alpha)$	$(3/2)(1-\alpha)^{2/3}(1-(1-\alpha)^{1/3})$	$(1-(1-\alpha)^{1/3})^2$
Three-dimensional diffusion model (Ginstein-Brounshtein equation)	$D_4(\alpha)$	$(3/2)((1-\alpha)^{-1/3}-1)$	$(1-2\alpha/3)-(1-\alpha)^{2/3}$
Chemical reaction controlled model (infinite plate)	$F_0(\alpha)$	1	α
Random nucleation model	$F_1(\alpha)$	1-α	$-\ln(1-\alpha)$
Chemical reaction controlled model (shrinking cylinder)	$R_2(\alpha)$	$2(1-\alpha)^{1/2}$	$1-(1-\alpha)^{1/2}$
Chemical reaction controlled model (shrinking sphere)	$R_3(\alpha)$	$3(1-\alpha)^{2/3}$	$1-(1-\alpha)^{1/3}$
Two-dimensional nuclei growth model (Avrami-Erofe'ev (m=2) equation)	$A_2(\alpha)$	$2(1-\alpha)(-\ln(1-\alpha))^{1/2}$	$(-\ln(1-\alpha))^{½}$
Three-dimensional nuclei growth model (Avrami-Erofe'ev (m=3) equation)	$A_3(\alpha)$	$3(1-\alpha)(-\ln(1-\alpha))^{2/3}$	$(-\ln(1-\alpha))^{1/3}$

1.6.1 The Friedman (FR) method

After taking the natural logarithm of each side of Equation (1.4), the model-free (isoconversional) Friedman's equation (FR) given in Equation (1.7) is obtained.

$$\ln\left(\beta.\frac{d\alpha}{dT}\right) = \left(-\frac{E_a}{R.T}\right) + \ln\ \left(A.f(\alpha)\right) \quad (1.7)$$

By this way "E_a" can be obtained for a particular "α" from the negative slope of the straight line showing the variation of "ln [β ($\frac{d\alpha}{dT}$)]" against "1/T" for different heating rates without making any assumption on the reaction model (Dilmaç 2021 marmara).

1.6.2 Flynn-Wall-Ozawa (FWO) method

The integral model-free Flynn-Wall-Ozawa (FWO) method uses Doyle's approximation for the solution of "p(u)". According to this method, linear fitting of "ln(β)" versus "1/T" couples obtained at different heating rates for a particular conversion (α) gives a straight line with a slope of "-1.051 E_a/R" as seen on Equation (1.8).

$$\ln(\beta) = \ln\left(\frac{A.E_a}{R.g(\alpha)}\right) - 5.331 - 1.051.\left(\frac{E_a}{R.T}\right) \quad (1.8)$$

1.6.3 Kissinger-Akahira-Sunose (KAS) method

The integral model-free Kissinger-Akahira-Sunose (KAS) method employs Murray and White approximation for the solution of "p(u)". According to this method "E_a" can be calculated from the slope of the straight line by plotting "ln(β/T^2)" versus "1/T" couples obtained at different heating rates for a particular "α" as seen in Equation (1.9).

$$\ln\left(\frac{\beta}{T^2}\right) = \ln\left(\frac{A.R}{g(\alpha).E_a}\right) - \frac{E_a}{R.T} \quad (1.9)$$

1.6.4 The Coats-Redfern (CR) method

The Coats-Redfern (CR) is one of the most popular methods used for model-fitting of the non-isothermal kinetic data. It employs asymptotic series expansion for approximating "p(u)" and yields Equation (1.10).

$$\ln\left(\frac{g(\alpha)}{T^2}\right) = \ln\left[\frac{A.R}{\beta.E_a}.\left(1-\frac{2.R.T}{E_a}\right)\right] - \frac{E_a}{R.T} \qquad (1.10)$$

Plotting "$\ln[g(\alpha)/T^2]$" versus "1/T" gives "E_a" and "A" from the slope and intercept respectively. The model that gives the best linear fit among the equations given in Table 1.2 is selected as the reaction model representing the mechanism (Ebrahimi-Kahrizsangi and Abbasi 2008).

1.7 Aim of the Study

The significance of this study rests in its attempt to use Tunçbilek lignite coal to potentially reduce nickel and iron oxides in Gördes laterite ore. Turkey is the eighth-largest producer of steel worldwide and has noticeable amount of laterite reserves. Due to the fact Ni and Fe significantly support the growth of Turkey's industrial sector and meet industrial needs, the process of extracting minerals from laterite ore is of utmost importance. The aim of this study was to extract nickel from lateritic ores obtained in Turkey's Gördes (Manisa) region. Extracting nickel from laterite ore by traditional methods requires high energy, with environmental pollution, by emitting polluting gases into the atmosphere at a high cost.

The current study examines the possibility of reduction of iron and nickel oxides in non-isothermal TGA conditions with less energy and the emission of polluting gases in smaller quantities. And the economic cost of this process is lower compared to traditional methods. Also the reaction kinetics is enlightened.

2. LITERATURE REVIEW

Since 1867, when the rich nickel silicate deposits of New Caledonia were discovered, nickel extraction from laterites has received attention (Li 1999).

There was a lot of variation between the kinetic model and activation energy values in the 1920s, particularly in experiments intended to figure out reduction kinetics. The emergence of this condition involved the successful use of a wide variety of experimental factors, including file configuration, lowering the gases used in experiments, and the chemical and physical properties of the ore, particle sizes, operating temperature, and types of reactors. For all of these reasons, there is a vast amount of literature about the study that is being presented, especially in this section and in relation to coal and H_2. We'll provide the findings of a recent study (Conard et al. 1978) that used gases and coal. The type of the reducing environment, the ratio of reductant to oxide, and temperatures between 350 and 850 °C were all studied. The final ferronickel alloy's nickel grade and nickel metallization were both governed by the reducing potential. While reducing hydrogen, the nickel grade increased along with the water concentration in the initial reducing environment. Additionally, when the water content increased, the amount of nickel that reported to the spinel phase decreased, and wustite predominated in more reducing conditions. If pure hydrogen or carbon monoxide were used, the majority of the nickel was reported to the alloy. Therefore, to reduce all nickel oxide, it would be most efficient to operate close to the stoichiometric need.

Energy is needed in large quantities to produce ferronickel from nickel laterite ore, especially when the ore has a low nickel content. Pre-treatment methods for laterite ore include selective reduction-beneficiation to remove gangue minerals and obtain nickeliferous concentrate with a high nickel concentration. Nickel laterite ores were selectively reduced using a mixture of 6% calcium sulfate and 5% reductant coal by Zhua *et al.* (2012) at 1100 °C for 60 minutes. To separate the reduced ore, wet magnetic separation was employed. According to experiments, it is possible to obtain a nickeliferous concentrate with a high nickel content of 6.0% Ni and a nickel recovery of

92.1% by discarding about 75% of the reduced ore with a low nickel concentration. The studies findings showed that silica concentration and the reduction environment have the biggest effects on reduction selectivity. According to the microscopic study, nickel oxide had diminished and nickel had mostly enriched into a Fe-Ni phase. Sulfur boosted Ni enrichment in metallic phases and accelerated the growth of Fe-Ni particles from 5.8 μm to 16.1 μm when sulfur was present.

Lv *et al.* (2017) used high purity carbon powder at 3 heating rates (10, 15 and 20 ^{o}C/min) from ambient temperature to 1773 K (1500 ^{o}C) in a thermal gravimetric analyzer under Ar atmosphere to non-isothermally reduce the calcined laterite ore from the Philippines (20 mg with 1.81% Ni and 17.87% Fe). According to the conversion levels = 0 - 0.40, =0.40 - 0.70, and = 0.70 - 0.9, the reduction process may be separated into three steps, with mean "E_a" values of 60 kJ/mol, 137 kJ/mol, and 383 kJ/mol, respectively. Chemical reaction was controlled throughout the first stage, but understanding of the second and third stages was insufficient for Masterplot interpretation.

Lv *et al.* (2018) performed the aforementioned reduction process by graphite using the same ore under the same experimental conditions. They employed the KAS approach for kinetic analysis and tracked the reduction's extremely changing activation energy, which suggests multistep reduction. The reduction process was split into three stages according to the conversion as low, medium, and advanced reduction levels based on the reaction rate graph. For further kinetic information, the Coats-Redfern approach was used to each stage. It was found that the first and second stages were regulated by diffusion, whereas the last stage was controlled by a chemical reaction.

Zhang *et al.* (2020) used a coal-based direct reduction process to separate ferronickel from low-grade nickel laterite ore. In nickel-bearing laterite ore pellets, the effects of basicity on compressive strength, metallization rate, microstructure, and reduction characteristics were investigated. The results of the study show that iron metallization and pellet compressive strength increase with increasing basicity. To prevent the formation of rings, the optimal reduction temperature for the rotary kiln should be

between 1150°C and 1250°C with a pellet basicity of 0.56. Ferronickel ([Fe, Ni]), forsterite, ferroan, and pigeonite make up the majority of metallized pellets when processing conditions are ideal.

3. MATERIAL AND METHOD

3.1 Laterite Ore and Tunçbilek Lignite

The laterite ore samples used in this study were supplied from Gördes (Manisa, Türkiye) mine via Meta Nickel Cobalt Company (META NİKEL KOBALT A.Ş.). The coarse ore pieces were crushed in a jaw breaker and sieved using standard sieves. Fine ore fractions with diameters smaller than 100 μm were used in experiments. The ore samples were calcined at 900 ºC for 18 hours in a muffle furnace to obtain more durable and mechanically resistant particles. The XRF chemical composition of the raw laterite ore is given in Table 3.1. It is essential to underline that Fe_2O_3 and NiO composition of the calcined ore increased up to 46.50% and 3.51% respectively due to the losses during calcination.

Table 3.1 Chemical composition of Gördes laterite ore

Fe_2O_3	Al_2O_3	SiO_2	NiO	CaO	Cr_2O_3	MgO	SO_3	Other
42.31	8.82	33.11	3.19	3.66	1.67	2.22	0.5	4.52

The lignite samples were supplied from Tunçbilek mines via General Directorate of Turkish Coal Enterprices (Türkiye Kömür İşletmeleri Kurumu A.Ş). After drying, crushing and sieving procedure, fine lignite fractions smaller than 100 μm were reserved for the experiments. The approximate and ultimate analysis of the dried Tunçbilek lignite is given in Table 3.2.

Table 3.2 Proximate and ultimate analysis of Tunçbilek lignite

Proximate Analysis % w/w, Dry basis	Volatile	Fixed Carbon	Moisture	Ash	Lower heating value (MJ/kg)
	36.40	41,80	0	21.79	24.44
Ultimate Analysis % w/w, Dry basis	C	H	N	S	O	Ash
	62.85	4.54	2.61	1.08	6.85	21.79

3.2 Experimental Set-up

The carbothermic reduction experiments within the scope of this study were carried out in the thermogravimetric analyzer (TA Instruments SDT Q600) shown in Figure 3.1.

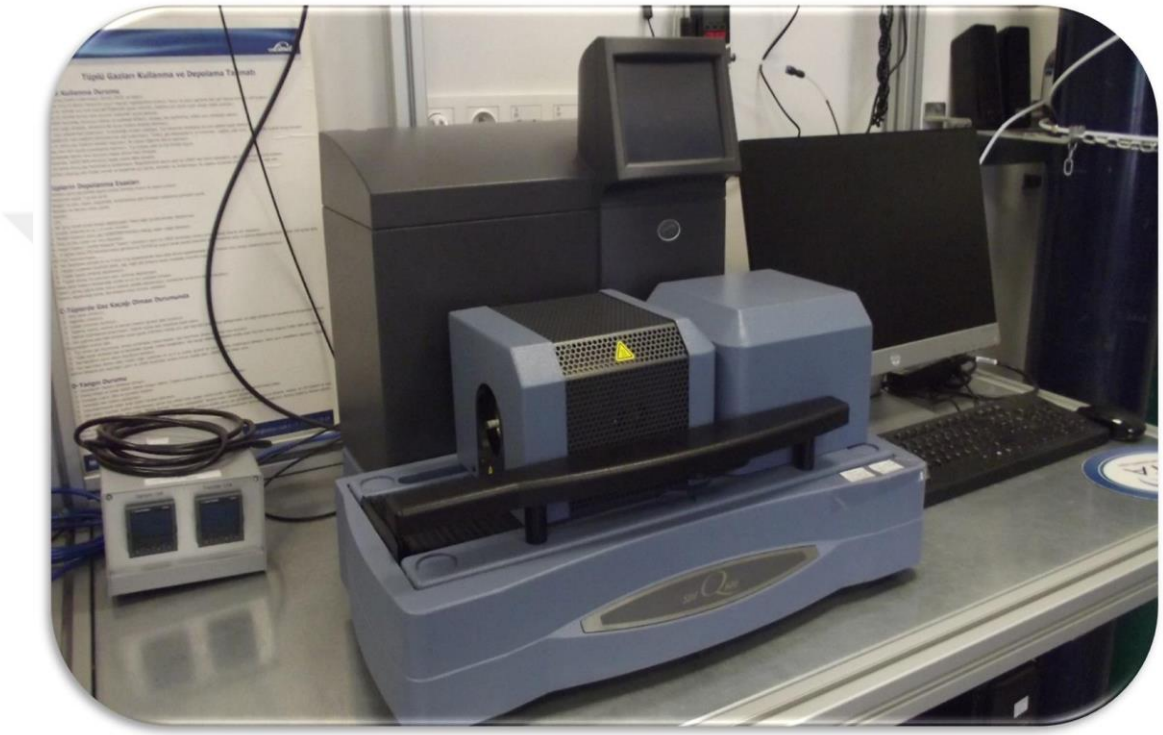

Figure 3.1 Experimental set-up

The calcined ore and lignite samples were mixed in a stoichiometric ratio (87% calcined ore and 13% dried lignite by mass) considering the minimum reductant requirement for the complete reduction of the iron and nickel oxides in the ore into their metallic forms. After obtaining a homogenous mixture, approximately 30 mg of sample was placed into an alumina crucible and heated in the TGA analyzer from ambient temperature to 1000 ºC under 20 ml/min. of N_2 flow. The experiments were performed at 5 different heating rates; 5, 10, 15, 25, and 40 ºC/min. All experiments were repeated for the same amount of lignite keeping all other parameters the same. Since the laterite was calcined in the muffle furnace prior to the experiments, no discernible weight loss was observed in the

thermogram of the ore sample. That is why the experimental procedure included solely lignite and "lignite-laterite" mixtures.

3.3 Method

The reduction degree of the metallic oxides in the laterite ore was calculated according to the method described by Ubando *et al.* (2019). In this method, an imaginary TGA curve ($TGA_{theroretical}$) is created considering how the weight of the mixture would change with increasing temperature, in case there was no reaction between the ore and the lignite according to the Equation (3.1), where "TGA" and "y" correspond to the TGA curve and weight fraction, whilst the subscripts "L" and "T" demonstrate calcined laterite ore and Tunçbilek lignite, respectively.

$$TGA_{theoretical} = (TGA_L \times y_L) + (T_T \times y_T) \quad (3.1)$$

Afterwards, the difference between the theoretical curve and the real one ($TGA_{experimental}$) was calculated using Microsoft Excel. Since "$TGA_{experimental}$" includes both the effects of volatilization of the lignite and the reduction of the metal oxides, however "$TGA_{theroretical}$" includes solely the decreases caused by volatilization of the lignite, the gap between "$TGA_{theroretical}$" and "$TGA_{experimental}$" provides a measure for determination of the reduction degree as seen in Equation (3.2).

$$Reduction\ Degree\ (\%) = \frac{TGA_{theoretical} - TGA_{experimental}}{w_O} \times 100 \quad (3.2)$$

"w_O" seen in Equation (3.2) is the weight of the oxygen bounded to the metallic oxides in the calcined laterite sample.

4. RESULTS AND DISCUSSION

4.1 Thermograms

The weight loss curves of Tunçbilek lignite, and "lignite-laterite" mixtures obtained at different heating rates are given in Figure 4.1, Figure 4.2, Figure 4.3, Figure 4.4, and Figure 4.5, respectively. Owing to be calcinated before the experiments, practically no change was observed in the weight of the laterite samples during heating up to 1000 ºC under N_2 atmosphere. Thus, solely the the weight changes of lignite, and "lignite-laterite" mixtures were examined in the following sections.

As seen from Figure 4.1, Figure 4.2, Figure 4.3, Figure 4.4, and Figure 4.5, the lignite samples underwent approximately 39% weight loss at all heating rates which is in accordance with the volatile matter percent given in Table 3.2. On the other hand, the weight loss of "lignite-laterite" mixtures eventuated between 6.59% and 7.83% depending on the heating rate. Those losses emerged from both volatilization of the lignite, and as well, from the carbothermic reduction of the ore *i.e.* the removal of the oxygen from metallic oxides in the laterite as a result of interacting with lignite.

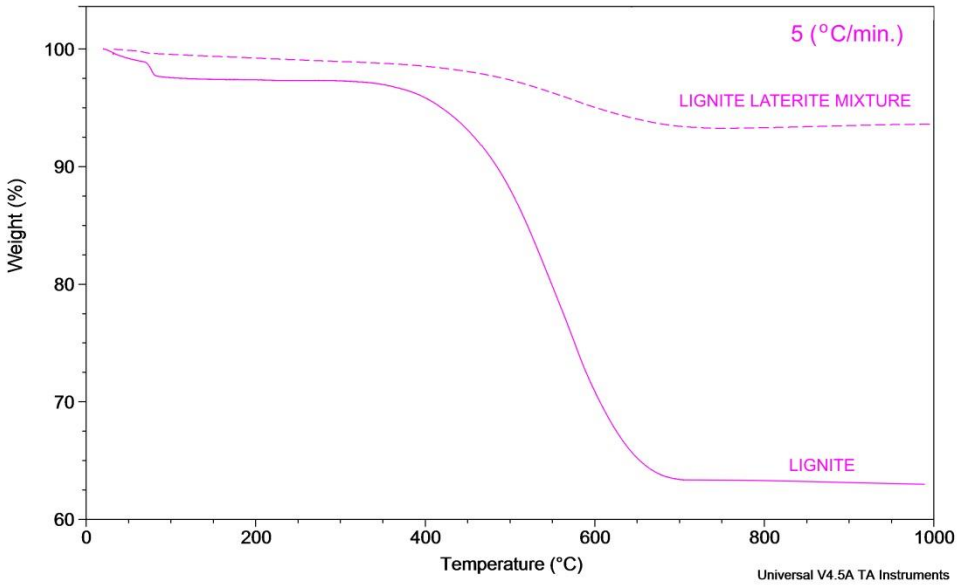

Figure 4.1 Weight loss of lignite and lignite-laterite mixture at 5 ºC/min. heating rate

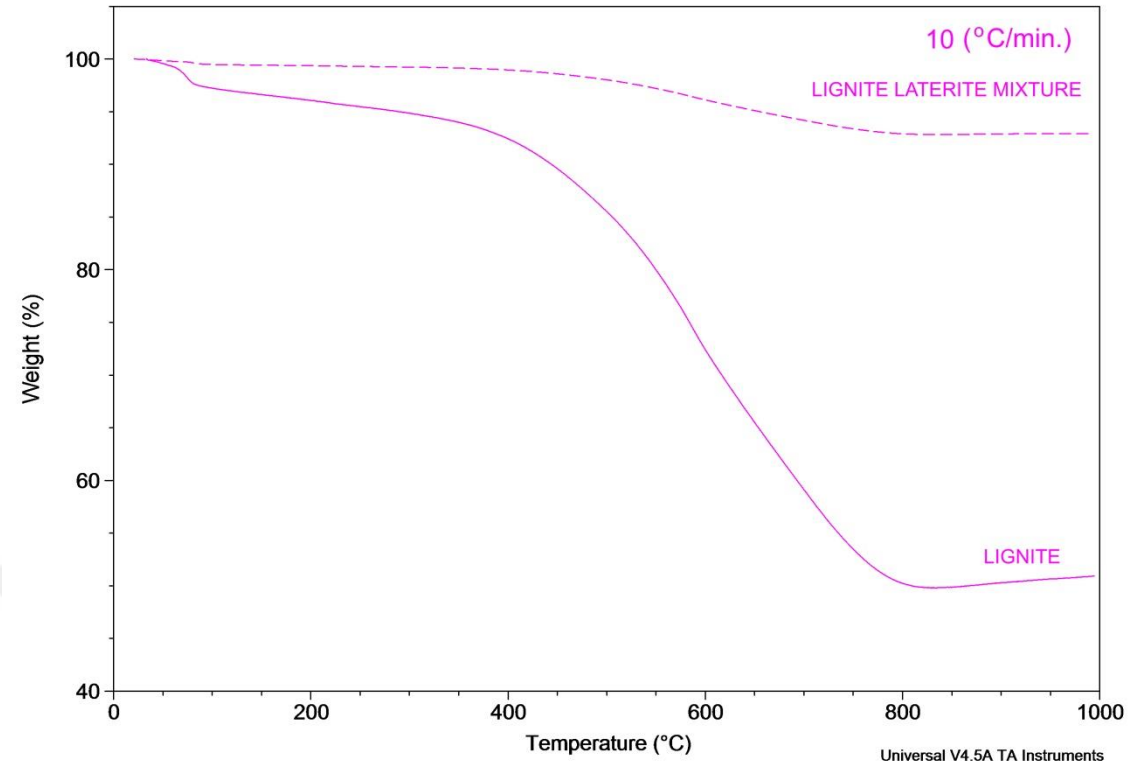

Figure 4.2 Weight loss of lignite and lignite-laterite mixture at 10 ºC/min. heating rate

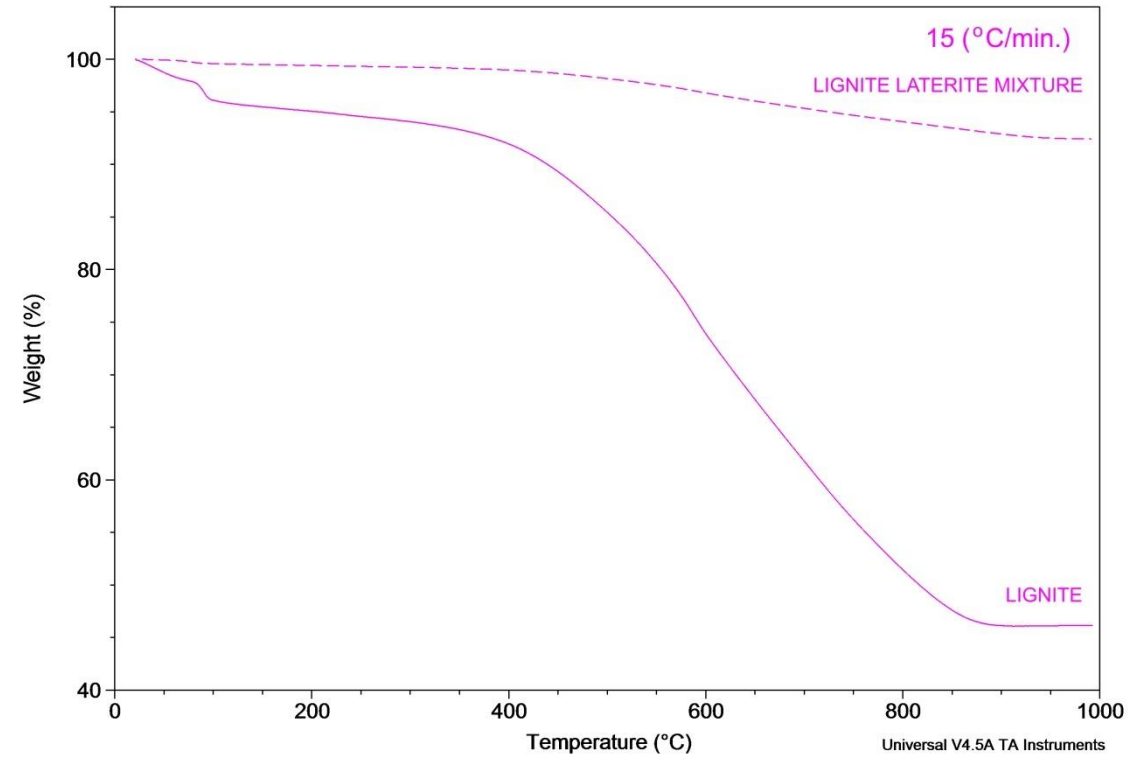

Figure 4.3 Weight loss of lignite and lignite-laterite mixture at 15 ºC/min. heating rate

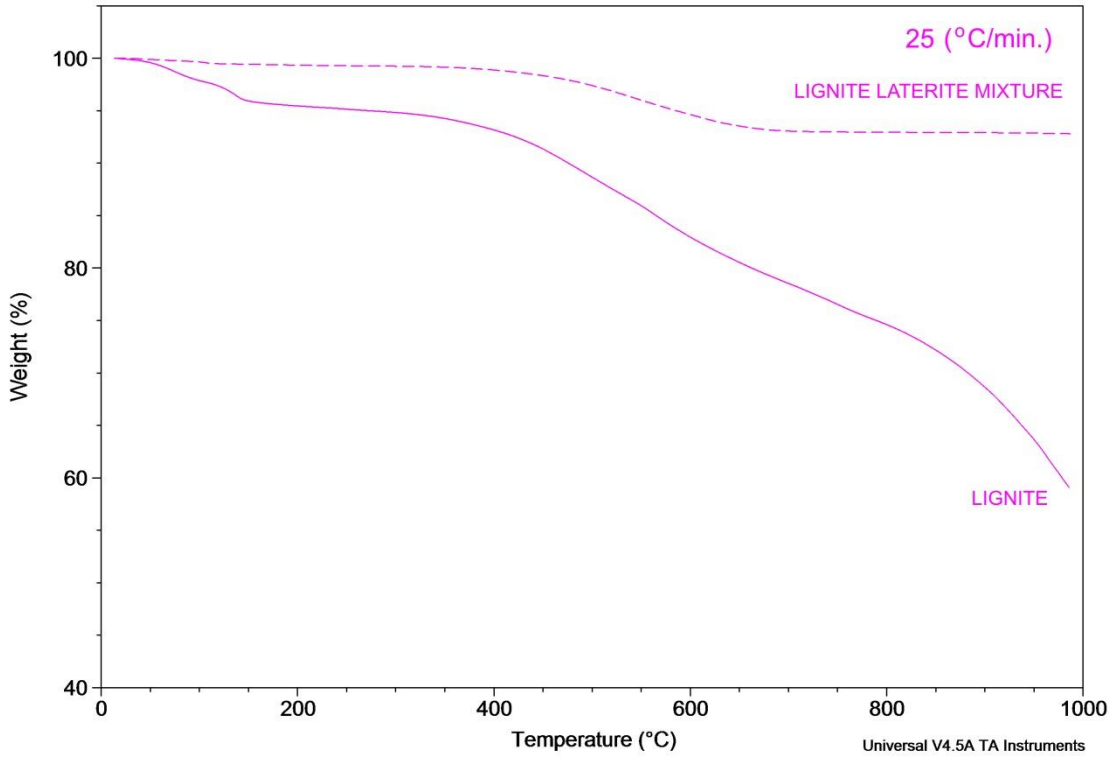

Figure 4.4 Weight loss of lignite and lignite-laterite mixture at 25 ºC/min. heating rate

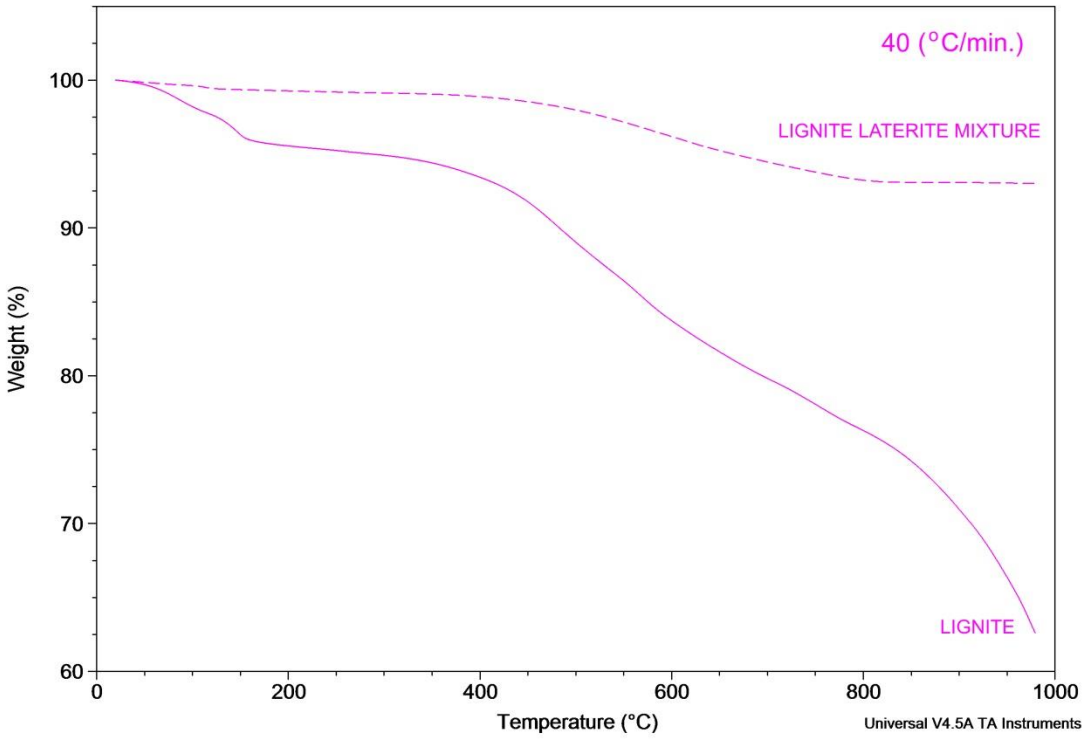

Figure 4.5 Weight loss of lignite and lignite-laterite mixture at 40 ºC/min. heating rate

4.2 Reduction Degree

The reduction degree of the calcined Gördes laterite samples by Tunçbilek lignite was calculated by the help of the TGA data according to the method explained in Section 3.3. The obtained results for various heating rates were graphed as seen in Figure 4.6.

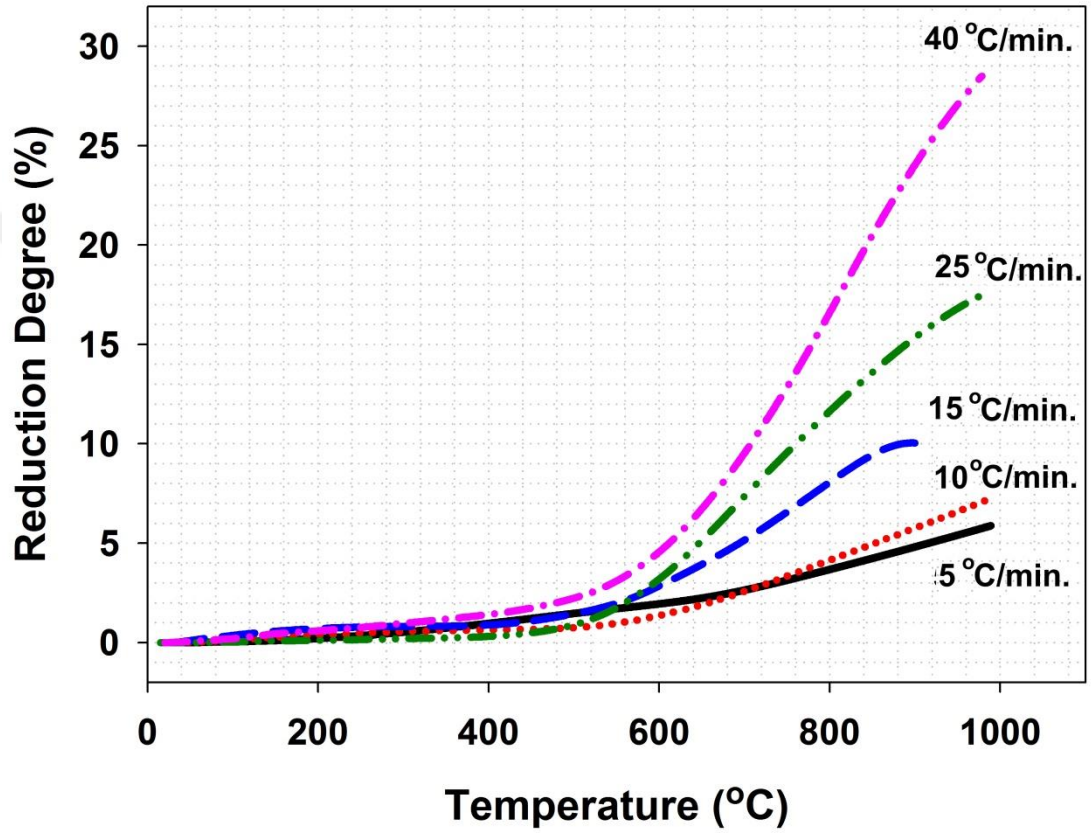

Figure 4.6 Variation of the reduction degree of the calcined laterite samples by Tunçbilek coal in TGA at various heating rates

As seen in Figure 4.6, the carbothermic reduction behavior of the laterite samples was highly sensitive to the heating rate, especially after 600 ºC, while maximum 29% reduction could be achieved at the highest heating rate most likely due to the low concentration of the lignite in the mixtures. These findings strengthen the argument that the reduction reaction occurred mostly under chemical reaction control.

4.3 Non-Isothermal Reduction Kinetics

Non-isothermal kinetic data obtained during the carbothermic reduction of calcined Gördes laterite by Tunçbilek lignite was firstly examined via various isoconversional methods such as; the differential model-free Friedman (FR) method, the integral model-free Flynn-Wall-Ozawa (FWO) method, and the integral model-free Kissinger-Akahira-Sunose (KAS) method to determine the activation energy of the process regardless of the model. The obtained graphs are given in Figure 4.7, Figure 4.8, and Figure 4.9 respectively. It should be kept in the mind that, since the abovementioned methods utilize the "conversion" instead of the "reduction degree", "α" which corresponds to one percent of the reduction degree was used for the further kinetic evaluations.

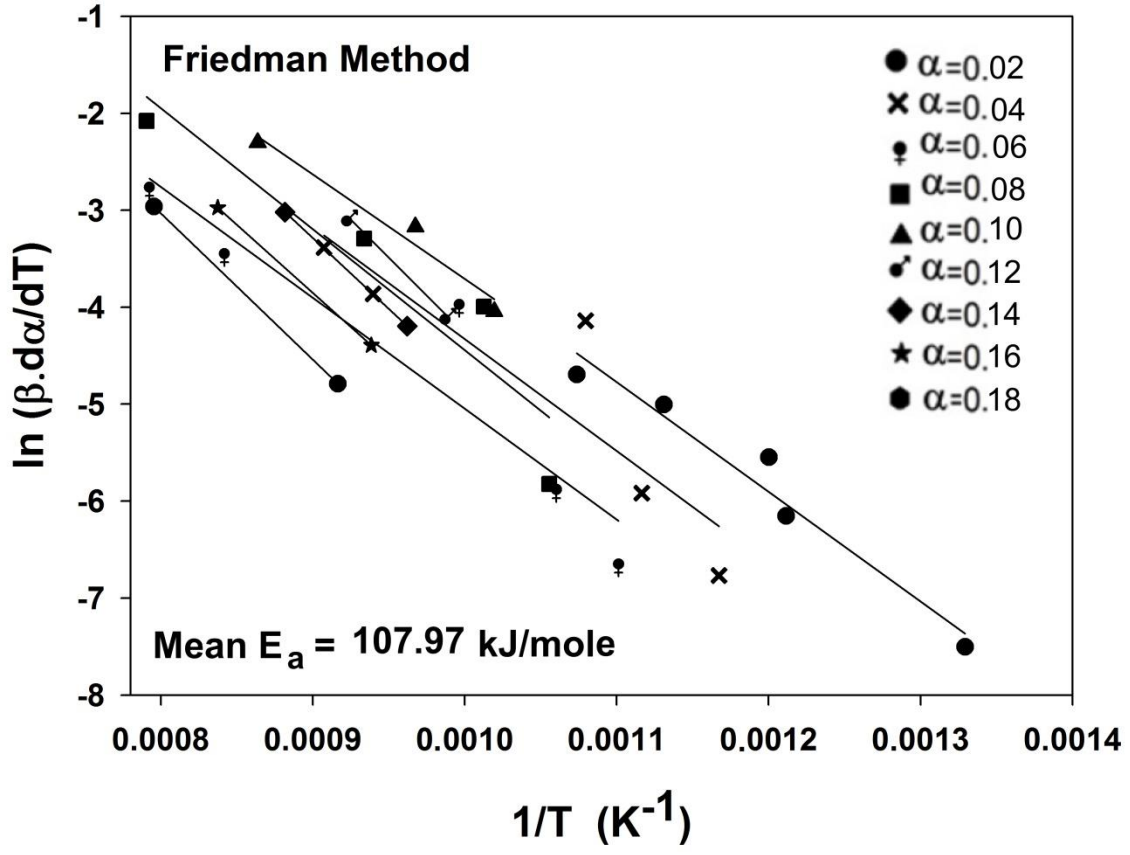

Figure 4.7 Determination of mean "E_a" for conversion levels between 0 and 0.18 using the Friedman method

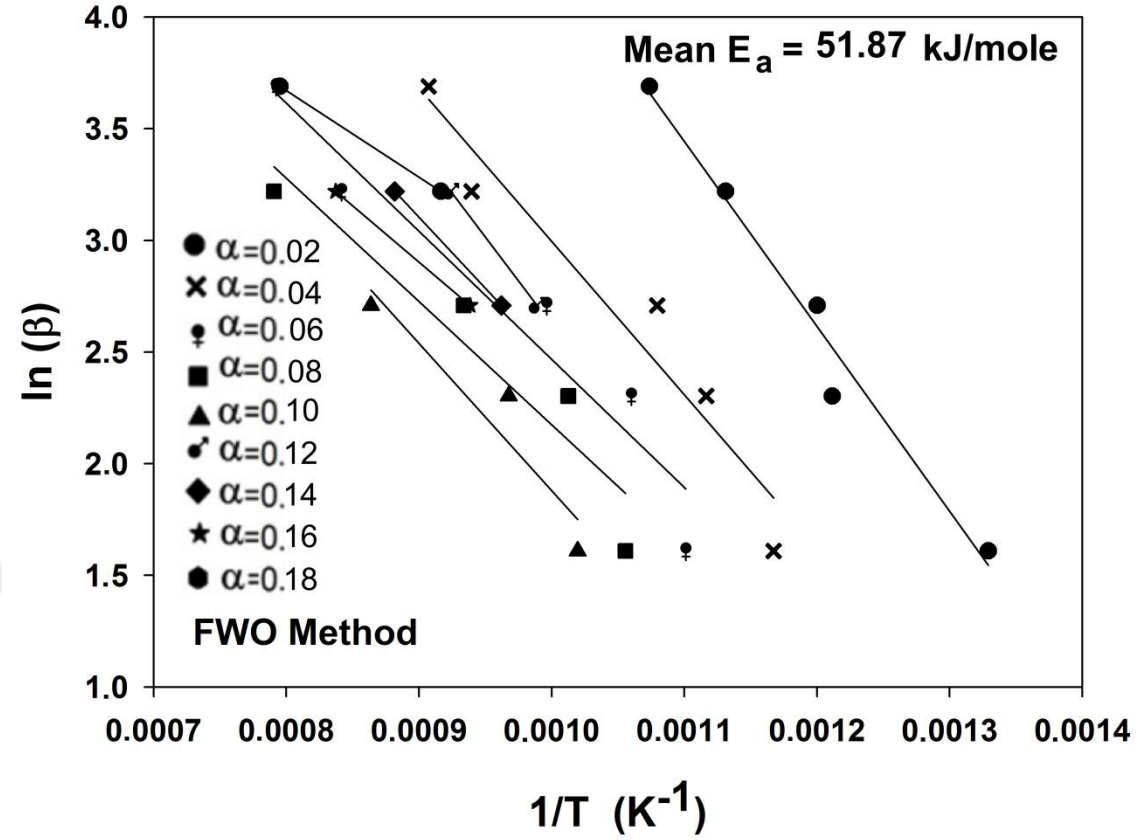

Figure 4.8 Determination of mean "E_a" for conversion levels between 0 and 0.18 using the Flynn-Wall-Ozawa (FWO) method

The mean E_a between 0 and 0.18 conversion during carbothermic reduction of calcined Gördes laterite by Tunçbilek lignite was determined as 107.97 kJ/mole, 51.87 kj/mole, and 63.67 kJ/mole via FR, FWO, and KAS methods, respectively. Two points should be emphasized based on the obtained results. First, the differential model-free Friedman (FR) method overestimated the mean E_a value (about 2 times), compared to the integral model-free Flynn-Wall-Ozawa (FWO), and Kissinger-Akahira-Sunose (KAS) methods as a common fact in the related literature.

Second, due to the low concentration of the lignite in the mixtures, the highest reduction was stricted as 29%, therefore, the mean "E_a" could be determined for a limited and low conversion range *i.e* for α values between 0 and 0.18.

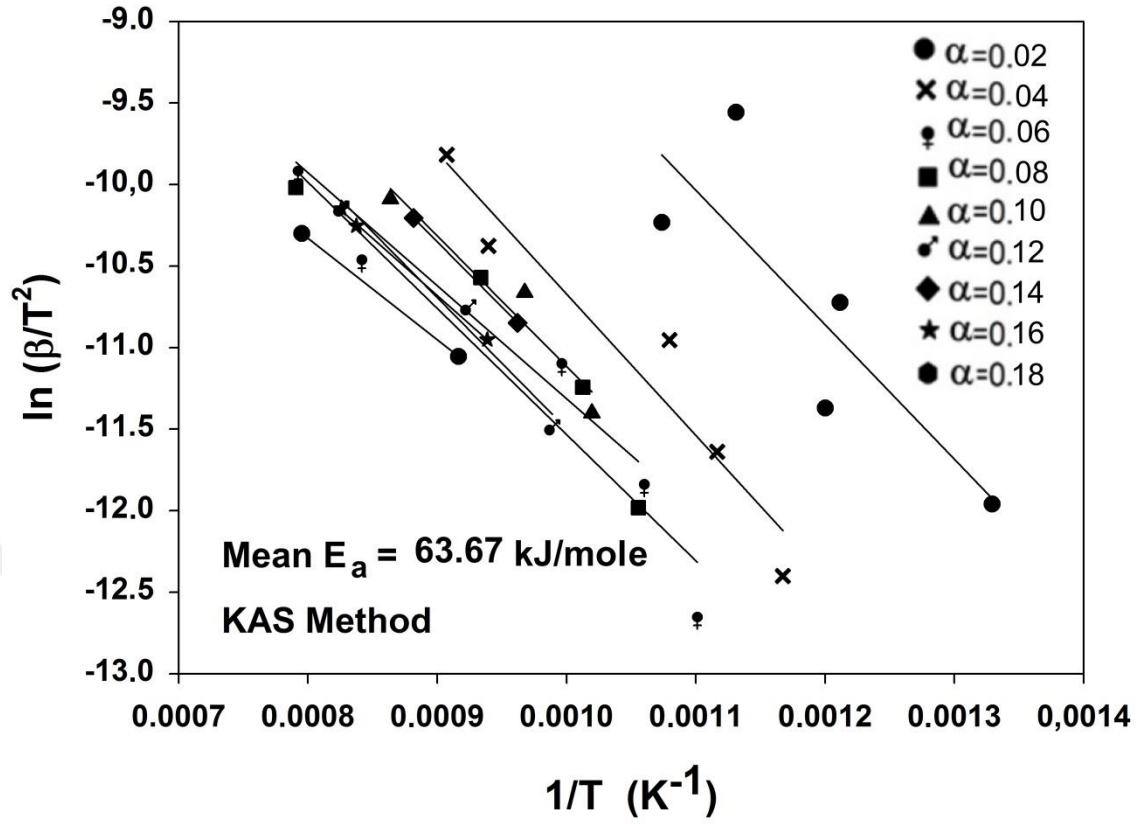

Figure 4.9 Determination of mean "E_a" for conversion levels between 0 and 0.18 using the Kissinger-Akahira-Sunose (KAS) method

After having an idea about the activation energy by the FR, FWO, and KAS methods, -albeit for a low conversion interval-, full kinetic analysis performed by using the Coats-Redfern method formulated by Equation (1.10). For that purpose, the non-isothermal "α vs t" data obtained at 40 ^oC/min. heating rate was converted into "$\ln[g(\alpha)/T^2]$" vs "1/T" graphs for all models given in Table 1.2. The best fitting model with the highest R^2, in other words the integral reaction model (g(α)) of the reduction process was determined as "F0" as seen in Figure 4.10. By this way, the kinetic triplet *i.e*, the rate controlling mechanism, the mean activation energy (E_a), and the Arrhenius frequency factor (A) was determined as; phase boundary chemical reaction control, 54.04 kJ/mole, and 0.49 $l^{n-1}.mole^{1-n}.s^{-1}$, respectively for the initial stages (between 0 and 0.29 conversion) of the carbothermic reduction of calcined Gördes laterite with Tunçbilek lignite.

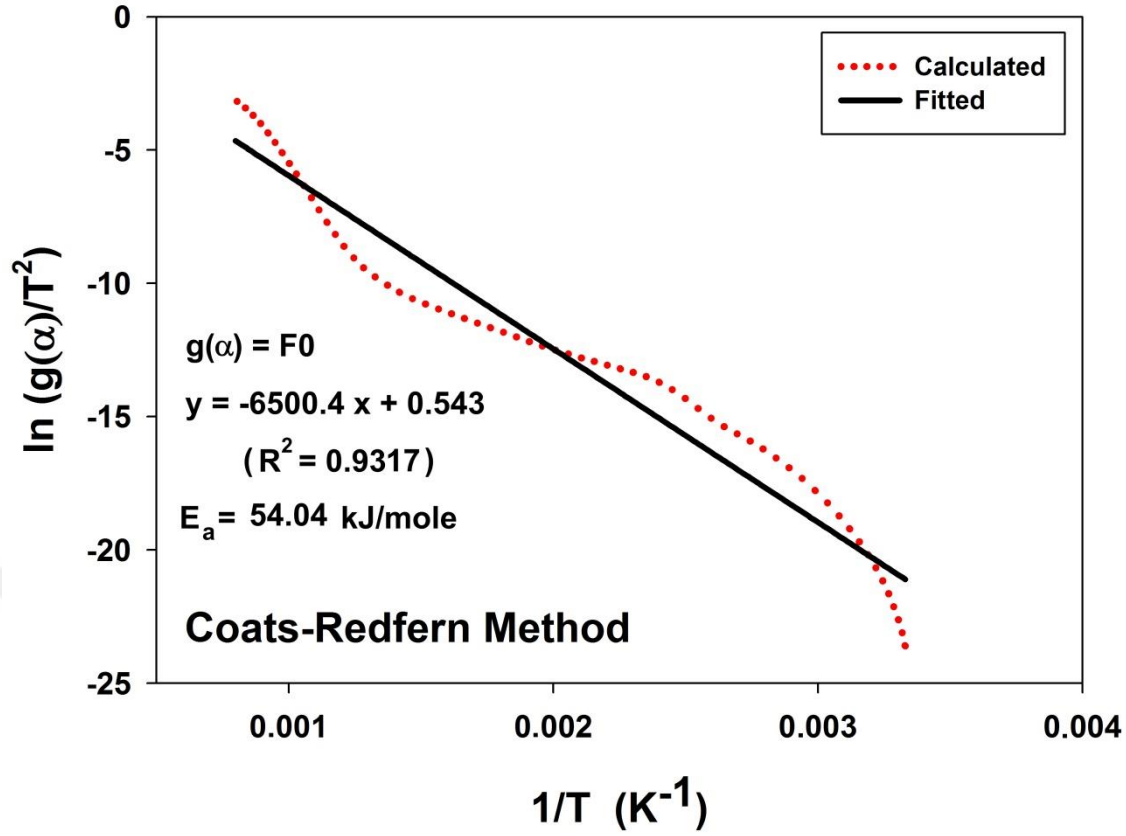

Figure 4.10 Determination of kinetic triplet using the Coats-Redfern (CR) method

5. CONCLUSIONS AND RECOMMENDATION

The main findings of this study can be summarized as follows;

1. Due to the low solid reductant concentration in laterite-lignite mixtures, the maximum reduction degree of metallic oxides in the ore stricted by approximately 29%. To enlight the full conversion mechanism of the metallic oxides in Gördes laterite into ferronickel, it is highly recommended to perform further experiments with higher lignite concentrations.

2. It was observed that as the heating rate increased, the weight loss and as well, the reduction degree of the "laterite- lignite" mixtures increased. The sensitivity of the reduction degree against the reductant concentration and the heating rate indicated that the first stages of the reduction took place under the control of the chemical reaction. In fact, it is unlikely that any product film exists that can control the rate of the process during the initial stages of reduction (between 0 and 0.29 conversions).

3. Isoconversional nonisothermal kinetic analysis of the TGA data revealed that the mean E_a between 0 and 0.18 extend during carbothermic reduction of calcined Gördes laterite by Tunçbilek lignite was as; 107.97 kJ/mole, 51.87 kj/mole, and 63.67 kJ/mole according to the FR, FWO, and KAS methods, respectively.

4. The kinetic triplet for the initial stages *i.e* 0 to 0.39 conversion levels, of the carbothermic reduction of calcined Gördes laterite with Tunçbilek lignite was identified by the model-fitting Coats-Redfern method. The phase boundary chemical reaction control characterized by "F0" integral model function was determined to be the controlling mechanism while, the mean activation energy (E_a), and the Arrhenius frequency factor (A) was calculated as 54.04 kJ/mole, and 0.49 $l^{n-1}.mole^{1-n}.s^{-1}$, respectively.

REFERENCES

Alsalihi, E. A. T. 2022. Menteş yöresi hematit cevherinin akışkan yatak reaktörde direkt indirgenme kinetiğinin belirlenmesi. MSc. Thesis, Çankırı Karatekin University, 52 pages, Çankırı.

BRITANNICA, 2023. Web site. https://www.britannica.com/science/nickel-chemical-element. Date of access: 01.05.2023.

Conard B.R., McAneney T.B. and Sridhar R. 1978. Thermodynamics of iron-nickel alloys by mass spectrometry. Metall. Mater. Trans. B-Process Metall. Mater. Process Sci., 9: 463–468.

Dilmaç, N. 2021. Non-isothermal reduction kinetics of Gördes laterite in CO atmosphere. Int. J. Adv. Eng. Pure Sci., 33(4):677-686.

EBAY, 2023. Web site. https://www.ebay.com/itm/224506493442. Date of access: 01.05.2023.

Ebrahimi-Kahrizangi, R. and Abbasi, M. H. 2008. Evaluation of reliability of Coats-Redfern method for kinetic analysis of non-isothermal TGA. Trans. Nonferrous Met. Soc. China, 18 (1): 217-221.

ELEMENTS, 2023. Web site. https://elements.visualcapitalist.com/the-worlds-largest-nickel-mining-companies/. Date of access: 01.05.2023.

Elias, M. 2002. Nickel laterite deposits-geological overview, resources and exploitation. University of Tasmania Special Publication, 4: 205-220.

Elliott, R. and Pickles, C. A. 2017. Thermodynamic analysis of the selective reduction of a nickeliferous limonitic laterite ore by hydrogen. High Temp. Mater. Proc., 36(8): 835-846.

Emiola-Sadiq, T., Zhang, L. and Dalai, A. K. 2021. Thermal and kinetic studies on biomass degradation via thermogravimetric analysis: a combination of model-fitting and model-free approach. ACS Omega, 6(34): 22233–22247.

Farooqui, A. E., Pica, A. M., Marocco, P., Ferrero, D., Lanzini, A., Fiorilli, S., Llorca, J. and Santarelli, M. 2018. Assessment of kinetic model for ceria oxidation for chemical-looping CO_2 dissociation. Chem. Eng. J., 346: 171-181.

Fedunik-Hofman, L., Bayon, A. and Donne, S. W. 2019. Kinetics of solid-gas reactions and their application to carbonate looping systems. Energies, 12 (15): 2981-3016.

Li, S. 1999. Study of nickeliferrous laterite reduction. MSc. Thesis, McMaster University, 163 pages, Ontario.

Li, B., Ding, Z., Wei, Y., Wang, H., Yang, Y., and Barati, M. 2018. Kinetics of reduction of low-grade nickel laterite ore using carbon monoxide. Metall. Mater. Trans. B-Process Metall. Mater. Process Sci., 49: 3067–3073.

LIVESCIENCE, 2023. Web site. https://www.livescience.com/29327-nickel.html. Date of access: 01.05.2023.

Liu, D. 2002. Recent development in nickel and cobalt recovery technologies from laterite. Nonferrous Metals (Extractive Metallurgy), 3: 6-10.

Lv, X., Lv, W., Wang, L., and Qiu, J. 2017. Thermal analysis kinetics of the solid-state reduction of nickel laterite ores by carbon. Miner. Met. Mater. Ser., 8: 147-160.

Lv, X., Lv,W., You, Z., Lv, X., and Bai, C. 2018. Non-isothermal kinetics study on carbothermic reduction of nickel laterite ore. Powder Technol., 340: 495-501.

Mcllveen, W. D. and Negusanti, J. J. 1994. Nickel in the terrestrial environment. Sci. Total Environ. 148(2-3): 109-138.

Meshram, P., Abhilash, D. and Pandey, P. D. 2019. Advanced review on extraction of nickel from primary and secondary sources. Miner. Process. Extr. Metall. Rev., 40 (3): 157-193.

METALS-HUB, 2023. Web site. https://www.metals-hub.com/blog/alloying-elements-in-steel-production/. Date of access: 01.05.2023.

NICKEL INSTITUTE, 2023. Web site. https://www.nickelinstitute.org/. Date of access: 01.05.2023.

NICKELSEARCH, 2023. Web site. https://nickelsearch.com/nickel/. Date of access: 01.05.2023.

Norgate, T. and Jahanshahi, S. 2011. Assessing the energy and greenhouse gas footprints of nickel laterite processing. Minerals Engineering, 24(7): 698-707.

PIPINGMART, 2023. Web site. https://blog.thepipingmart.com/metals/top-3-uses-of-nickel/. Date of access: 01.05.2023.

PUBCHEM, 2023. Web site. https://pubchem.ncbi.nlm.nih.gov/element/Nickel#section=Description. Date of access: 01.05.2023.

REUTERS, 2023. Web site. https://www.reuters.com/markets/commodities/like-musk-nickel-rich-indonesia-has-high-electric-vehicle-ambitions-2023-02-06/. Date of access: 01.05.2023.

STATISTA, 2023. Web site. https://www.statista.com/statistics/1245590/nickel-supply-worldwide/#:~:text=Global%20supply%20of%20nickel%202019%2D2023&text=The%20global%20supply%20of%20nickel,metric%20tons%20worldwide%20in%202023. Date of access: 01.05.2023.

Su, M., Ma, J., Tian, X. and Zhao, H. 2017. Reduction kinetics of hematite as oxygen carrier in chemical looping combustion. Fuel Process. Technol., 155: 160-167.

Ubando A.T., Chen W.H. and Ong H.C. 2019. Iron oxide reduction by graphite and torrefied biomass analyzed by TG-FTIR for mitigating CO_2 emissions. Energy, 180: 968-977.

Valix, M., Tang, J. Y. and Cheung, W. H. 2001. The effects of mineralogy on the biological leaching of nickel laterite ores. Minerals Engineering, 14(12): 1629-1635.

Wang, X., Sun, T., Chen, C., and Hu, T. 2017. Current studies of treating processes for nickel laterite ores, Advances in Computer Science Research, 70: 139-152.

WIKIPEDIA, 2023. Web site. https://en.wikipedia.org/wiki/Nickel. Date of access: 01.05.2023.

Yang, S., Du, W., Shi, P., Shangguan, J., Liu, S., and Zhou, C. 2016. Mechanistic and kinetic analysis of Na_2SO_4 -Modified laterite decomposition by thermogravimetry coupled with mass spectrometry. PLoS One, 11(6): 1-21.

Zhai, X., Fu, Y., Zhang, X., Ma, L. and Xie, F. 2009. Intensification of sulphation and pressure acid leaching of nickel laterite by microwave radiation. Hydrometallurgy, 99 (3-4): 189-193.

Zhang, Y., Cui, K., Wang, J., Wang, X., Qie, J., and Xu, Q. 2020. Effects of direct reduction process on the microstructure and reduction characteristics of carbon-bearing nickel laterite ore pellets. Powder Technol., 376: 496-506.

Zhou, Q. 2005. Current Situation and Development Direction of Technology for Oxidized Nickel Ore Treatment. Yunnan Metallurgy, 34(6): 33-36.

Zhu, D., Pan, L., Guo, Z., Pan, J., and Zhang, F. 2019. Utilization of limonitic nickel laterite to produce ferronickel concentrate by the selective reduction-magnetic

separation process. Adv. Powder Technol., 30: 451–460.

Zhua D., Pan L., Guo Z., Pan, J. and Zhang F. 2012. Utilization of limonitic nickel laterite to produce ferronickel concentrate by the selective reduction-magnetic separation process. Adv. Powder Technol., 30: 451–460.